Time-resolved and Site-specific Insights into Migration Pathways of Li+ in α-Li3VF6 by 6Li 2D EXSY NMR Spectroscopy

ARTICLE *in* THE JOURNAL OF PHYSICAL CHEMISTRY C · JULY 2010

Impact Factor: 4.77 · DOI: 10.1021/jp103433h

6 AUTHORS, INCLUDING:

Martin Wilkening
Graz University of Technology
119 PUBLICATIONS **1,564** CITATIONS
SEE PROFILE

Ekaterina E. Romanova
University of Southern California
11 PUBLICATIONS **121** CITATIONS
SEE PROFILE

Dominik Alexander Weber
Justus-Liebig-Universität Gießen
21 PUBLICATIONS **39** CITATIONS
SEE PROFILE

Paul Heitjans
Leibniz Universität Hannover
265 PUBLICATIONS **3,624** CITATIONS
SEE PROFILE

Time-Resolved and Site-Specific Insights into Migration Pathways of Li^+ in α-Li_3VF_6 by ^6Li 2D Exchange MAS NMR

M. Wilkening,*,† E. E. Romanova,†,‡ S. Nakhal,§ D. Weber,§ M. Lerch,§ and P. Heitjans†

Institut für Physikalische Chemie und Elektrochemie, Zentrum für Festkörperchemie und Neue Materialien (ZFM), Leibniz Universität Hannover, Callinstr. 3a, 30167 Hannover, Germany, Institut für Experimentelle Physik I, Universität Leipzig, Linnéstr. 5, 04103 Leipzig, Germany, and Institut für Chemie, Technische Universität Berlin, Str. des 17. Juni 135, 10623 Berlin, Germany

Received: April 16, 2010; Revised Manuscript Received: July 15, 2010

Two-dimensional (2D) exchange nuclear magnetic resonance (NMR) spectroscopy carried out under magic angle spinning (MAS) conditions is ideally suited to study site-specific Li diffusion parameters of cathode materials required for the target-oriented development of so-called high-energy density 4 V-lithium-ion batteries. In the present study, we took advantage of Li NMR hyperfine shifts to record temperature-variable 1D and mixing-time dependent 2D exchange MAS ^6Li NMR spectra on α-Li_3VF_6 serving as both a potential cathode material as well as an application-oriented model substance with three magnetically inequivalent Li sites. By comparing the NMR results with structural details of the material we were able to obtain detailed insights into the migration pathways and Li exchange rates which are of the order of some hundreds of Li jumps per second at approximately 340 K. Site-specific Li jump rates τ^{-1} reveal the electrochemically active sites and provide information how to modify the material in order to increase its relatively low Li diffusivity found at room temperature.

Introduction

The atomic-scale measurement of dynamic processes such as the elementary steps of Li^+ hopping in ionically conducting solids is of great interest for the knowledge-based identification and/or development of materials showing a high mobility of their charge carriers. In particular, fast ion conductors are required, e.g., for the design of powerful and clean energy storage systems with high-energy density such as Li ion batteries[1−10] which are intended by many car manufacturers to be installed in electric vehicles in the near future.

Besides others, lithium metal fluorophosphates and metal fluorides[11−14] are regarded as very promising materials to act as so-called high-energy density 4 V-cathodes in rechargeable batteries. However, although an enormous number of papers dealing with solid-state diffusion exist, very few experimental studies can be found which take up the challenge to follow Li^+ ion migration in detail by using a microscopic method such as nuclear magnetic resonance (NMR) being unique in its possibilities for this purpose.[14−23] The first 2D magic angle spinning (MAS) exchange NMR experiment performed on a Li ion conductor was carried out by Stebbins and co-workers using polycrystalline lithium orthosilicate which served as a favorable model substance showing at least four well-resolved ^6Li NMR signals.[15] These NMR lines represent Li ions in Li_4SiO_4 which reside in the center of crystallographically different polyhedra characterized by distinct NMR chemical shifts. Succeeding ^6Li and ^7Li 2D MAS NMR studies,[14,16,18,24] which are based on this pioneering NMR experiment to probe Li dynamics, were mainly carried out on cathode materials containing transition metals with suitable redox couples (e.g., Mn or V).

In general, the diffusion parameters of paramagnetic compounds, being particularly characterized by very broad NMR lines and extremely short Li spin−lattice relaxation (SLR) times, are hardly measurable by time-domain NMR techniques such as recording spin−spin or spin−lattice rates[20,25−28] as well as Li stimulated echoes.[29−38] These difficulties are caused by the interaction between the magnetic moment of the Li spins with the much larger one of the unpaired electrons leading to strong background effects dominating NMR spin−lattice relaxation rates and, thus, masking any diffusion-controlled contributions. However, in most cases the Fermi-contact delocalization interaction between the unpaired d-electrons at the transition metal centers and the lithium nuclei[39] leads to site-specific hyperfine $^{6,7}Li$ NMR shifts which can be well resolved under magic angle spinning conditions.[14,16,18,21−23] This enables the use of high-resolution multidimensional NMR experiments in order to shed light on the Li exchange processes in such materials from a microscopic point of view.

In the present study the cathode material α-Li_3VF_6, crystallizing in the same space group as its diamagnetic counterpart α-Li_3AlF_6,[40] is used as an application-oriented model substance to reveal the Li hopping processes by 2D exchange NMR in detail and to relate the findings to the crystallographic structure of the material.

Experimental Section

α-Li_3VF_6 was prepared by reacting stoichiometric amounts of LiF and VF_3 at 800 °C in a monel capsule for 2 h. The sample was then quenched by removing the capsule out of the furnace. Phase analysis was carried out by means of X-ray powder methods using a Siemens D 5000 diffractometer (Bragg−Brentano geometry, $CuK_{\alpha 1}$ radiation). A subsequent Rietveld refinement

* Corresponding author. E-mail: wilkening@pci.uni-hannover.de. Web: www.wilkening.pci.uni-hannover.de. Phone: +49 511 762 3273. Fax: +49 511 762 19121.
† Leibniz Universität Hannover.
‡ Universität Leipzig.
§ Technische Universität Berlin.

10.1021/jp103433h
Published on Web 09/14/2010

TABLE 1: Atomic Positions for α-Li_3VF_6

atom	*x*	*y*	*z*
V(1)	0.126(1)	0.2471(1)	0
F(1)	0.234(3)	0.060(2)	0.143(6)
F(2)	0.027(2)	0.230(2)	0.355(4)
F(3)	0.246(2)	0.238(2)	0.677(4)
F(4)	0.015(3)	0.409(2)	0.852(7)
F(5)	0.245(3)	0.371(2)	0.172(5)
F(6)	0.020(3)	0.089(2)	0.830(6)
Li(1)	0.375	0.349	0.507
Li(2)	0.105	0.457	0.497
Li(3)	0.354	0.546	0.002

gives 2% unreacted VF_3 as secondary phase. α-Li_3VF_6 crystallizes in the orthorhombic system with the following lattice parameters: $a = 959.12(2)$ pm, $b = 848.85(2)$ pm, $c = 503.82(1)$ pm. In analogy to the well-known crystal structure of α-Li_3AlF_6, see ref 40, space group $Pna2_1$ was chosen for the Rietveld procedure. The refined atomic parameters are given in Table 1. X-ray methods are not sensitive enough for a trustworthy determination of the Li positions. Consequently, we used the Li positions known from α-Li_3AlF_6 which were not refined.

^{6}Li MAS NMR spectra were recorded at a high magnetic field of 17.6 T corresponding to a resonance frequency of 110.4 MHz. A wide-bore Bruker Avance-750 spectrometer in combination with a standard Bruker MAS probe, supporting rotors of 4.0 mm in outer and 2.4 mm in inner diameter, was used for the NMR measurements. NMR spectra were recorded at spinning frequencies of up to 15 kHz and referenced to 1 M LiCl (aq) (0 ppm). They were acquired with a single 90° preparation pulse with a length of 3.6 μs and a recycle delay of 0.3−5 s. Up to 500 scans were accumulated for one spectrum. 2D exchange NMR spectra were recorded using a NOESY pulse sequence[41] at different mixing times ranging from 1 to 80 ms. For one 2D NMR spectrum 200 scans were accumulated with time domains of 128 and 1024 data points in the F1 and F2 direction, respectively. Rotation synchronized acquisition was performed in both F2 and F1 directions using dwell times of 1/15 ms. States-TPPI and phase correction in F1 direction were used to obtain the 2D spectra. ^{6}Li NMR spin−lattice relaxation times were determined using a standard inversion recovery pulse sequence.[42]

Results and Discussion

α-Li_3VF_6 (space group $Pna2_1$, see above), whose crystal structure is depicted in Figure 1, has three unique crystallographic Li sites fully occupied by Li^+. Vanadium cations (shown in dark gray) are octahedrally coordinated by six fluorine anions (blue). The three crystallographically different and magnetically inequivalent Li cations (labeled as Li(1), Li(2), and Li(3)) reside in octahedral voids which are connected to each other by face sharing as highlighted in Figure 1. The Li sites are well resolved by 1D ^{6}Li MAS NMR, see the NMR spectrum of Figure 2a), which was recorded under ambient bearing gas temperature. The NMR signals, which are characterized by distinctly different chemical shifts, are labeled with A, B, and C. Li(1) occupies the middle position of the triplet Li(2)−Li(1)−Li(3) which is shown in Figure 3 in detail, including also the internuclear Li−Li distances and the area of the triangular face shared by neighbored LiF_6-octahedra. While Li(1) and Li(3) have access to several migration paths to leave the triplet and to enter another one (see below), there is only one possibility for Li(2) to leave its initial site and to enter an unoccupied one of Li(3)′ which belongs to a new triplet. The

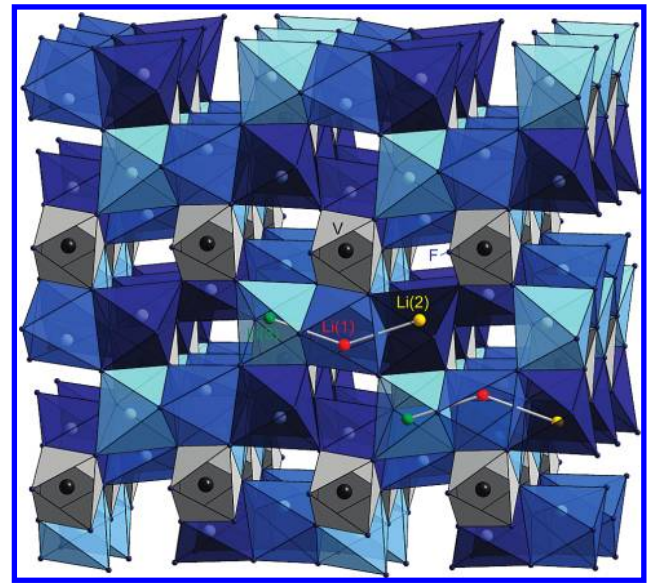

Figure 1. Crystal structure of α-Li_3VF_6 with the viewing direction along the *c*-axis. Dark gray spheres denote V^{3+} cations, and the blue ones represent fluorine anions. Some of the Li cations Li(1), Li(2) and Li(3) are highlighted by red, yellow, and green spheres, respectively.

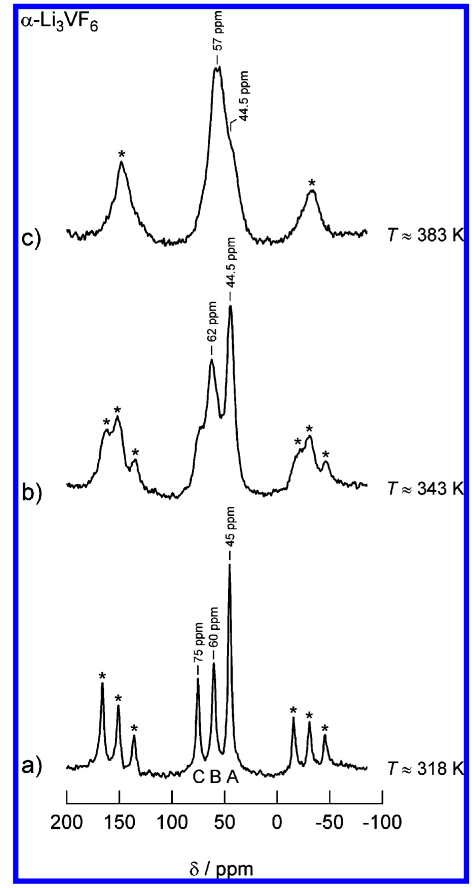

Figure 2. Temperature-variable 1D ^{6}Li MAS NMR spectra of α-Li_3VF_6 recorded at a nominal field of 17.6 T corresponding to a ^{6}Li NMR resonance frequency of approximately 110.4 MHz. The rotation frequency was 10 kHz.

triplets Li(2)−Li(1)−Li(3) themselves are connected to each other only by shared corners or edges. Thus, within the α-Li_3VF_6 structure only two direct exchange processes via octahedra sharing common faces are possible: Li(1) can directly exchange with Li(3) or with Li(2). In both cases the jump distance is

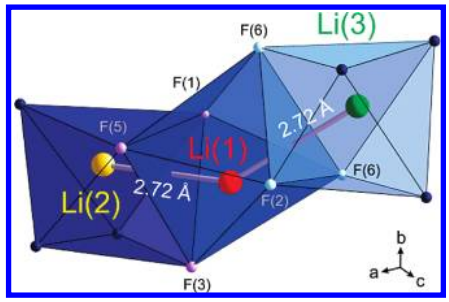

Figure 3. Triplet Li(2)−Li(1)−Li(3) in α-Li_3VF_6. The octahedra shown are connected sharing common faces. The triangular faces between Li(1) and Li(3) as well as Li(1) and Li(2) are highlighted by fluorine anions represented by light blue (F(6)−F(2)−F(6)) and light pink spheres (F(1)−F(5)−F(3)), respectively. The corresponding areas differ only marginally and amount to 3.78 and 3.83 $Å^2$, respectively.

relatively short and less than 2.8 Å (see Figure 3). In fact, the ^{6}Li MAS NMR spectrum of Figure 2b, recorded at a temperature *T* which is by approximately 30 K higher than that of the spectrum shown in Figure 2a, clearly reveals line broadening which is unambiguously caused by cation exchange between the distinct Li sites. At even higher temperatures full coalescence is observed (Figure 2c). It is worth noting that compared with the spectrum of Figure 2a the outer NMR signals of Figure 2b exhibit a larger decrease in intensity when compared to that of the NMR signal showing up at approximately 60 ppm. Therefore, one of the most probable exchange processes involving face-shared LiF_6-octahedra, i.e., either Li(1) ↔ Li(3) or Li(1) ↔ Li(2), is somewhat faster than the other one. This is unequivocally corroborated by 2D exchange ^{6}Li NMR experiments presented below.

Prior to discussing the 2D NMR results one can try to assign the ^{6}Li NMR resonances A, B, C with their almost equidistant hyperfine shifts to the lattice sites Li(1), Li(2), and Li(3). The NMR shifts result from the Fermi-contact interaction which is proportional to the transfer of electron spin density from the V^{3+} t_{2g} orbital (the electron configuration of V^{3+} is $t_{2g}^2e_g^0$) to the 2s one of the Li cation, see, e.g., refs 14, 18, 39, 43, and 44 for details. The more electron spin density is transferred, the more the NMR lines are shifted to higher resonance frequencies, i.e., in the direction of positive ppm values.

In the case of V^{3+} positive electron spin density can be transferred via the delocalization mechanism in two ways (see Figure 4). Li can receive spin-density of the same polarization either directly by overlapping of the t_{2g} orbital of the octahedrally coordinated transition metal with the 2s orbital of an Li atom in an edge-sharing octahedron or from the t_{2g} orbital through the F $2p_\pi$ one to the Li 2s orbital. For the latter the most effective transfer occurs when the angle included by the orbitals takes a value of 90° ($t_{2g}-2p_\pi-2s$ hybridization). The more the angle deviates from this ideal geometric configuration, i.e., the poorer the orbital overlap, the less spin density is transferred. In the case of V^{3+} with $t_{2g}^2e_g^0$ electron configuration the usually weaker polarization mechanism (Figure 4) takes advantage of a 180° interaction for the transfer of negative electron spin density (polarization of $e_g-2p_\sigma-2s$ orbitals) leading to a low-frequency NMR shift. However, in α-Li_3VF_6 nearly all the Li−F−V angles substantially deviate from 180° so that this transfer mechanism plays a minor role for the correct assignment of the NMR resonances. Let us mention that for Li(1) one angle Li(1)−F−V of about 150° is found which might cause a slight shift of the corresponding NMR signal toward negative ppm values.

Since it is not practicable to refine the exact Li coordinates from X-ray powder diffraction data (see above) and corresponding neutron diffraction data are not available yet, the following discussion is used as a rough estimate for the observed NMR hyperfine shifts, only. While Li(1) has five vanadium centers in its second coordination sphere (Figure 5a), Li(2) and Li(3) are exposed to only four nearest-neighbor V^{3+} cations (Figure 5b,c). However, most of the Li(1)−F−V bond angles deviate from 90° and range between 120 and 155°. Moreover, they are characterized by relatively long Li(1)−V distances of about 3.5 Å. The $Li(1)F_6$-octahedra are connected to four VF_6-octahedra by corner sharing only and to the fifth one by edge sharing. In the latter configuration electron spin density can be transferred via the orbitals including an angle close to 90°. However, the Li−V distance is somewhat larger than those for the Li(2) and Li(3) ions which are, moreover, each connected to two VF_6-octahedra by edge sharing (Figure 5b,c). Regarding the bond angles of Li(2)−F−V and Li(3)−F−V as well as the respective interatomic distances the decisive differences to decide which of the two Li cations benefits from the largest electron spin density are relatively small suggesting that the NMR signal corresponding to Li(3) should be adjacent to that of Li(2). For both Li sites, Li(2) and Li(3), an Li−F−V angle of approximately 95° is found. However, the Li−F and Li−V distances of the $Li(3)V_6$-octahedron is by about 0.2 Å smaller than those for Li(2). While Li(2) is connected to a VF_6-octahedron via a second angle of ca. 97°, the Li(3) site benefits from electron spin density transfer via an Li−F−V angle very close to 90°. Moreover, the latter is characterized by a rather short Li−V distance of approximately 3 Å. Taken together, based on these rough estimations taking into account polyhedra connectivity, bond angles as well as interatomic distances, one comes to the following, to our opinion most probable, assignment: Li(1) corresponds to the NMR line observed at the lowest frequency (signal A, 45 ppm), while Li(3) with its very short Li−M distances shows the largest frequency shift (site C, 75 ppm). Consequently, the NMR resonance of Li(2) is recorded at 60 ppm (site B) which is thus adjacent to the NMR line of Li(3). The same assignment is found when the fractional coordinates of fully refined Li_3AlF_6 is used.[40] Even when the

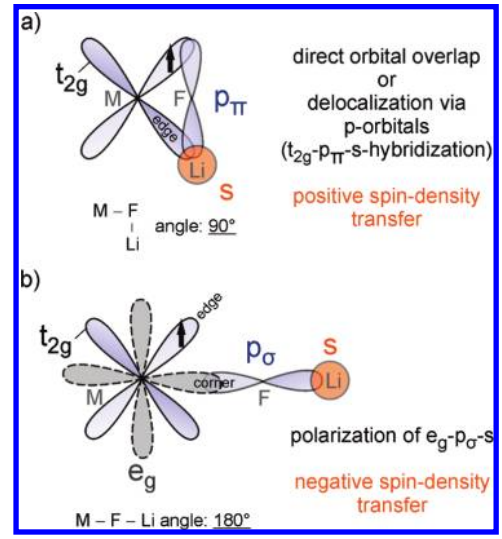

Figure 4. Schematic illustration showing how spin-density can generally be transferred from the metal cation (M) by the (a) delocalization mechanism as well as (b) polarization mechanism (see text for further details). For example, in the case of V^{3+} positive spin-density is transferred by the delocalization mechanism from the t_{2g} orbital to the 2s Li orbital either by direct orbital overlap (octahedral configuration with edge-sharing polyhedral VF_6 and LiF_6, see also Figure 5) or by involving the F $2p_\pi$ orbitals. The latter is most effective for an Li−F−V angle of 90°.

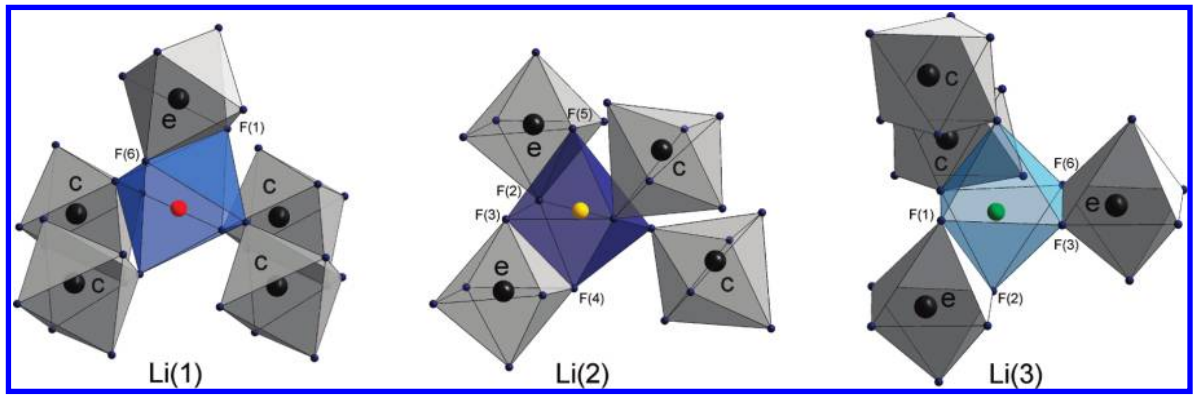

Figure 5. Number of vanadium ions in the coordination sphere of Li(1), Li(2), and Li(3). Most of the electron spin density is transferred via edge-shared (labeled with e) VF_6-octahedra rather than by those which are connected to the LiF_6-octahedra by corner sharing (labeled with c). The fluorine anions F(k) with $k = 1...6$ connect the 2s orbital of the Li nuclei with the d orbitals of the V cations. Regarding the interatomic distances and the bond angles included by the Li, F, and V atoms, the hyperfine NMR shift increases according to the following order: Li(1) < Li(2) < Li(3).

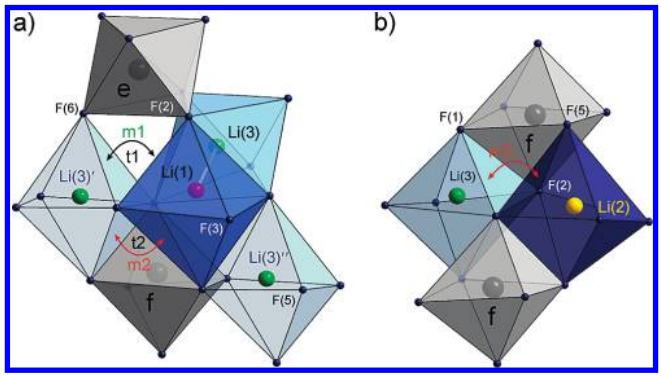

Figure 6. Possible two-step hopping mechanisms (m1, m2, and m3) in α-Li_3VF_6 for (a) Li(1) and Li(3) as well as (b) Li(2) and Li(3) to exchange via the empty tetrahedral positions t1 and t2, respectively. Dark gray spheres represent V cations. Mechanism m1 is energetically favored compared to m2 and m3. The VF_6-octahedron connected to the octahedra Li(1)F_6 and Li(3)″F_6 by edges (e) involving F(3) and F(5) is omitted for clearness. Li(1)F_6-octahedra are connected to Li(2)F_6 octahedra by sharing common edges, only.

positions x, y, z of Li ions are slightly shifted to larger or lower values, the site of Li(3) turned out to be the position with the highest and Li(1) that with the lowest frequency shift.

With respect to this assignment the dynamic process mainly affecting the changes of the temperature-variable 1D ^{6}Li NMR spectra of Figure 2b can be identified with the Li(1) ↔ Li(3) exchange. This seems to be reasonable when the following structural details are considered being independent of the exact Li positions and highlighting further connectivities of the two LiF_6-octahedra. Li(1) ions can reach Li(3) sites and vice versa not only directly by using a one-step diffusion path but also by taking advantage of a two-step or curved migration pathway. These include Li^+ hopping involving several unoccupied tetrahedral sites connecting the Li(1)F_6- and Li(3)F_6-octahedra by face sharing. The structural details are shown in Figure 6. Altogether there are four migration pathways for Li(1) to reach two different unoccupied Li(3)′ positions of neighbored Li(2)−Li(1)−Li(3) triplets due to the circumstance that the Li(1)F_6-octahedra of a triplet share their edges with two adjacent Li(3)F_6-octahedra. For example, Li(1) can reach the empty Li(3)′-site of Figure 6 via pathway m1 or m2. It is obvious that the first migration path (m1) is energetically favored as the repulsive Li^+-V^{3+} interaction is smaller when entering the tetrahedron t1. This tetrahedron is connected via F(2) and F(6) to a neighbored VF_6-octahedron by edge instead of face sharing being the case when path m2 is considered by the Li(1) ion. The same holds for the Li(3)″ site. In Figure 6a the corresponding hopping mechanisms m1′ and m2′ have been omitted for the sake of brevity and clearness. Altogether, there are two possibilities (m1 and m1′) for Li(1) and Li(3) to exchange and to leave the triplets Li(2)−Li(1)−Li(3) via interstitial positions acting as intermediately occupied Li sites or, most likely, as energetically favored transition states. This is in contrast to the situation for the Li(2)F_6-octahedron sharing, besides its connection to Li(1) in the triplet Li(2)−Li(1)−Li(3), only one edge with another Li(3)F_6-octahedron (see Figure 6b). However, the two tetrahedra built by the two octahedra Li(2)F_6 and Li(3)F_6, respectively, are connected to the neighbored VF_6-octahedra by face sharing. When using one of these migration pathways (m3 and m3′) the Li ions are temporarily exposed to short Li−V-distances.

Let us note that most probably a transient occupation of the tetrahedral sites discussed above might not be detectable in the 2D EXSY NMR experiments performed to trace slow Li dynamics. However, at much higher temperatures the involvement of intermediately occupied sites might show an influence on the fully coalesced 1D NMR spectra recorded on nonrotating as well as on rotating samples since the occupation probability and effective residence time of the Li ions is large enough to exert an influence on the NMR spectra. Moreover, instead of a "temporary occupation" simply a curved migration pathway involving the free volume of the tetrahedral sites might play a decisive role. This should not necessarily lead to a new detectable signal in the 2D NMR spectra. However, the different nondirect migration pathways accessible by the Li ions and discussed above might lead to distinct and site-specific jump rates.

In summary, taking into account also nondirect or two-site diffusion pathways, the Li jump rate $\tau_{1\leftrightarrow 3}^{-1}$ is expected to be larger than $\tau_{1\leftrightarrow 2}^{-1}$ which is in turn larger than $\tau_{2\leftrightarrow 3}^{-1}$. Such details are hardly to extract from temperature-variable ^{6}Li MAS NMR spectra showing coalescence of all NMR signals at sufficiently high temperatures from which a mean value for the Li jump rate can be roughly estimated. In the present case above 390 K the mean jump rate should reach a value of the order of $\pi\nu/\sqrt{2}$ where ν is the separation of the NMR resonance lines before any exchange occurred. Inserting $\nu \approx 3340$ Hz this yields approximately 7.4×10^4 s^{-1} for the mean hopping rate. Of course, at ambient temperature this rate is expected to be much lower. In contrast to 1D NMR, by the use of mixing-time

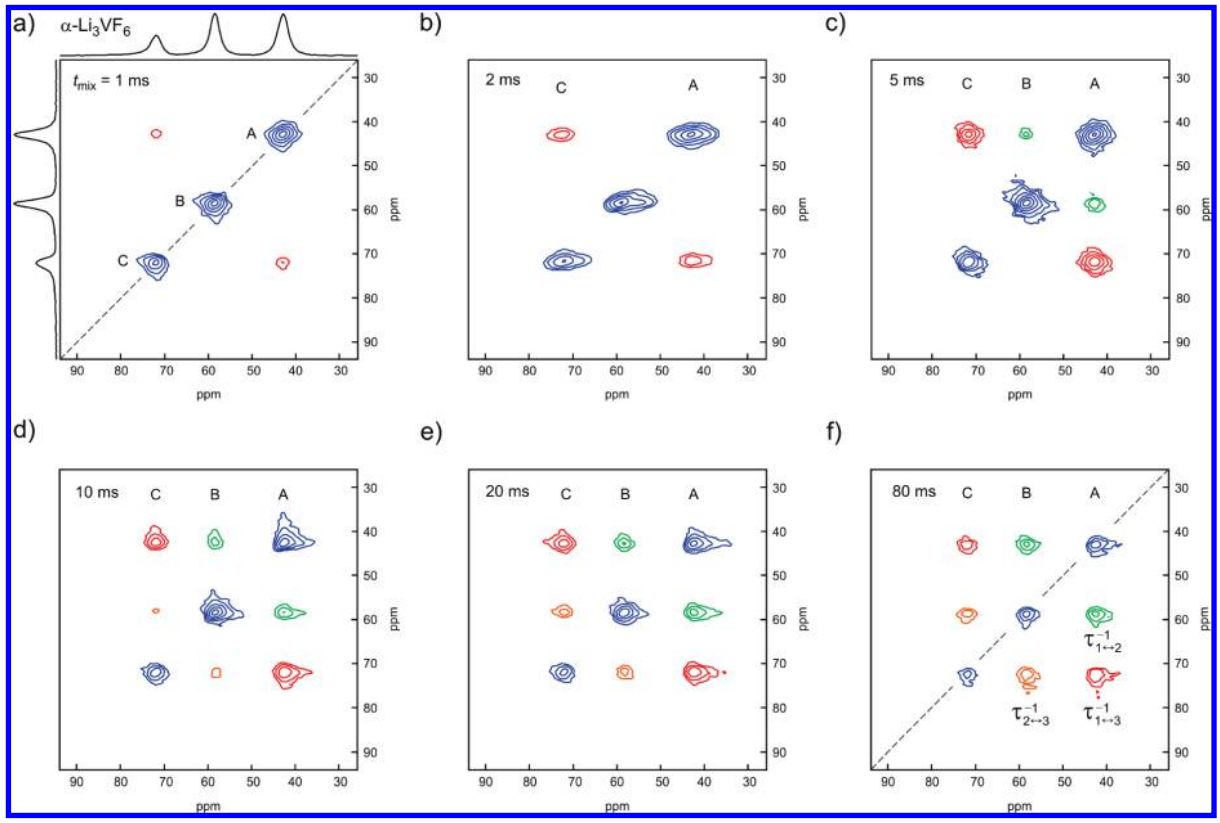

Figure 7. Rotor-synchronized 2D ^{6}Li MAS NMR spectra of α-Li_3VF_6 measured at ambient bearing gas pressure at a spinning speed of 15 kHz and an external magnetic field of 17.6 T. The spectra were recorded for the mixing times t_m indicated ranging from 1 to 80 ms. The corresponding ^{6}Li NMR spin−lattice relaxation time is about $T_1 = 80$ ms determining, in the present case, the upper limit of 2D exchange NMR experiments.

dependent two-dimensional exchange NMR experiments much deeper insight into the dynamic processes is obtainable and, in particular, site-resolved information on exchange processes can be determined. In Figure 7 high-resolution 2D ^{6}Li MAS NMR spectra are shown which were recorded at a spinning speed of 15 kHz and at approximately 340 K when taking into account the temperature rise due to spinning of the rotor. Exchange processes can be directly studied by analyzing the appearance of cross-peaks (off-diagonal peaks) and the increase of their (normalized) intensities as a function of mixing time.[41] In a 2D NMR experiment, the angular NMR frequency $\omega(t')$ of a given cation at time t' is correlated with the frequency $\omega(t'')$ after a mixing time t_m. Off-diagonal intensities result if $\omega(t') \neq \omega(t'')$, i.e., when jumps between magnetically inequivalent sites occur during t_m, Apart from chemical exchange, cross peaks may also show up because of spin-diffusion. However, in the present case such an influence seems to be negligible since a sample with natural isotope abundance (only 7.5% ^{6}Li) was used for the NMR measurements shown here ensuring a sufficiently good spatial separation of the ^{6}Li spins.

In perfect agreement with the interpretation of the 1D NMR spectra, exchange between sites A and C is seen first, i.e., already at a mixing time t_m of only 1 ms. This is more pronounced when t_m is increased to 2 ms. The relevant cross peaks are shown in red. According to the discussion presented above, this might correspond to the Li exchange process Li(1) ↔ Li(3). A further increase of t_m by a factor of only 2.5 reveals exchange occurring between A and B (shown in green) which most likely mirrors hopping of Li(1) and Li(2). It is clear from this experiment that signal A should be identified with Li(1), otherwise the second exchange process becoming visible would correspond to Li hopping between sites 3 and 2. Such an exchange process is less favored and not possible via a one-step jump process through face-sharing octahedra (vide supra). Even when only this assumption is taken into account and the above-mentioned assignment of the hyperfine shifts is disregarded, there is only one of six possibilities left to assign the signals A, B, C in a different way: signal A still corresponds to Li(1), but B and C represent Li(3) and Li(2), respectively. However, regarding the discussed migration pathways of Figure 6 it seems to be most likely that direct exchange between sites Li(1) and Li(3) is a little bit more favored compared to hopping between sites 1 and 2. Clearly, the probability that via m1 and m1′ vacancies are formed located at the regularly Li sites 1 and 3 is larger than that for Li(2). Certainly, it is expected that Li(1) ↔ Li(2) exchange is seen in the 2D NMR plots at a mixing time slightly larger than 2 ms. Increasing t_m to 10 ms a third exchange process becomes evident which finally corresponds to the dynamic processes of Li(2) and Li(3). In conclusion, on the basis of these considerations, in Figure 7c the site-specific rates are assigned to their respective off-diagonal intensities. Thereby, no indications for self-exchange processes are seen at the time scales and temperature of our experiments. This is entirely plausible due to the fact that crystallographically identical Li sites in α-Li_3VF_6 are connected by edge-shared LiF_6-octahedra, only.

Finally, a quantitative analysis of the rates is possible when the cross-peak intensities, which are normalized to the sum of the intensities of the diagonal peaks (for each mixing time t_m), are plotted as a function of t_m (see Figure 8). Assuming an exponential buildup of the normalized cross-peak signal intensities according to $I_{rel.} \propto 1 - \exp(-r_{i\leftrightarrow j} t_m)$ (lines in Figure 8) yields the following site-specific (first-order) jump rates $r_{i\leftrightarrow j} = \tau_{i\leftrightarrow j}^{-1}$ being in agreement with the above-mentioned prediction: $\tau_{1\leftrightarrow 3}^{-1} = 225\ s^{-1}$, $\tau_{1\leftrightarrow 2}^{-1} = 49\ s^{-1}$, and $\tau_{2\leftrightarrow 3}^{-1} = 31\ s^{-1}$. Thus, the hopping rate $\tau_{1\leftrightarrow 3}^{-1}$ is by a factor of approximately 7 larger than

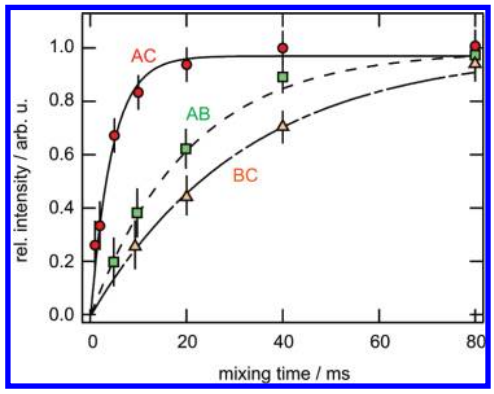

Figure 8. Normalized intensities of the AC, AB and BC cross peaks as deduced from the two-dimensional ^{6}Li MAS NMR spectra of α-Li_3VF_6 which were recorded (see Figure 7) as a function of mixing time. The lines show fits using a single exponential function $I_{rel.} \propto 1 - \exp(-r_{i\leftrightarrow j}t_m)$ with $r_{i\leftrightarrow j} = \tau^{-1}_{i\leftrightarrow j}$ to obtain site-specific Li hopping rates.

$\tau^{-1}_{2\leftrightarrow 3}$. Compared to other Li ion conductors studied by NMR and being relevant for Li batteries[18,20,24,27] Li diffusion in α-Li_3VF_6 is rather slow at ambient temperatures. This might be due to the circumstance that the number density of vacant Li sites is rather small prohibiting fast exchange processes. Preliminary NMR measurements on delithiated $Li_5V(PO_4)_2F_2$ by Makimuara et al. have shown that Li exchange increases when Li is partially removed from the structure.[14] Expectedly, this might be also the case for α-Li_3VF_6.

Summary and Conclusion

High-resolution one and two-dimensional ^{6}Li MAS NMR was used to enlighten diffusion pathways and hopping rates of Li cations in orthorhombic α-Li_3VF_6 representing with its three unique Li sites an interesting model system to study elementary Li jump processes from a microscopic point of view. In combination with structural considerations the multidimensional NMR data provided detailed insight into the Li exchange processes occurring on a millisecond time scale. Obviously, Li(1) and Li(3) ions are involved in the most favorable diffusion pathway. These ions are expected to be removed first during delithiation of α-Li_3VF_6 when used as a cathode material. Increasing the Li diffusivity might be possible by creating Li vacancies preferentially on the Li(1) or Li(3) sites in the Li(2)−Li(1)−Li(3) triplets. Since Li(2) sites are less involved in through-going, i.e., long-range diffusion, these are predestinated to be filled with, e.g., divalent cations in order to create Li vacancies on the desired positions. However, divalent cations residing on Li(1) or Li(3) sites are expected to impede Li diffusivity significantly.

Acknowledgment. We thank J. Heine and B. Ruprecht of our workgroup in Hannover as well as D. Freude (University of Leipzig) for fruitful discussions. We gratefully acknowledge financial support of the BMBF for this work within the frame of the project "High-energy lithium ion batteries (HE-Lion)". Furthermore, support by the DFG within the project "Avance 750 (Jürgen Haase)" is highly appreciated.

References and Notes

(1) Tarascon, J. M.; Armand, M. *Nature* **2001**, *359*, 1414.
(2) Nazar, L. F.; Goward, G.; Leroux, F.; Duncan, M.; Huang, H.; Kerr, T.; Gaubicher, J. *Int. J. Inorg. Mater.* **2001**, *3*, 191.
(3) Whittingham, M. S. *Chem. Rev.* **2004**, *104*, 4271.
(4) Bruce, P. G. *Solid State Sci.* **2005**, *7*, 1456.
(5) Aricò, A. S.; Bruce, P.; Scrosati, B.; Tarascon, J.-M.; Schalkwijc, W. V. *Nat. Mater.* **2005**, *4*, 366.
(6) Bruce, P. G.; Scrosati, B.; Tarascon, J.-M. *Angew. Chem., Int. Ed.* **2008**, *47*, 2930.
(7) Bruce, P. G. *Solid State Ion.* **2008**, *179*, 752.
(8) Whittingham, M. S. *Dalton Trans.* **2008**, 5424.
(9) Goodenogh, J. B.; Kim, Y. *Chem. Mater.* **2010**, *22*, 587.
(10) Ellis, B. L.; Tae Lee, K.; Nazar, L. F. *Chem. Mater.* **2010**, 691.
(11) Barker, J.; Saidi, M. Y.; Swoyer, J. L. *J. Electrochem. Soc.* **2003**, *150*, A1394.
(12) Li, H.; Balaya, P.; Maier, J. *J. Electrochem. Soc.* **2004**, *151*, A1878.
(13) Yin, S. C.; Herle, P. S.; Higgins, A.; Taylor, N. J.; Makimura, Y.; Nazar, L. F. *Chem. Mater.* **2006**, *18*, 1745.
(14) Makimura, Y.; Cahill, L. S.; Iriyama, Y.; Goward, G. R.; Nazar, L. F. *Chem. Mater.* **2008**, *20*, 4240.
(15) Xu, Z.; Stebbins, J. F. *Science* **1995**, *270*, 1332.
(16) Verhoeven, V. W. J.; de Schepper, I. M.; Nachtegaal, G.; Kentgens, A. P. M.; Kelder, E. M.; Schoonman, J.; Mulder, F. M. *Phys. Rev. Lett.* **2001**, *86*, 4314.
(17) Cabana, J.; Dupré, N.; Rousse, G.; Grey, C. P.; Palacín, M. R. *Solid State Ion.* **2005**, *176*, 2205.
(18) Cahill, L. S.; Chapman, R. P.; Britten, J. F.; Goward, G. R. *J. Phys. Chem. B* **2006**, *110*, 7171.
(19) van Wüllen, L.; Echelmeyer, T.; Meyer, H.-W.; Wilmer, D. *Phys. Chem. Chem. Phys.* **2007**, *9*, 3298.
(20) Wilkening, M.; Heitjans, P. *Phys. Rev. B* **2008**, *77*, 024311.
(21) Davis, L. J. M.; Heinmaa, I.; Goward, G. R. *Chem. Mater.* **2010**, *22*, 769.
(22) Murugesan, V.; Kerisit, S. N.; Wang, C. M.; Nie, Z.; Rosso, K. M.; Yang, Z.; Graff, G. L.; Liu, J.; Hu, J. Z. *J. Phys. Chem. C* **2009**, 14567.
(23) Vijayakumar, M.; Kerisit, S.; Yang, Z.; Graff, G. L.; Liu, J.; Sears, J. A.; Burton, S. D.; Rosso, K. M.; Hu, J. Z. *J. Phys. Chem. C* **2009**, *113*, 20108.
(24) Cahill, L. S.; Iriyama, Y.; Nazar, L. F.; Goward, G. R. *J. Mater. Chem.* **2010**, *20*, 4340.
(25) Heitjans, P.; Schirmer, A.; Indris, S. In *Diffusion in Condensed Matter - Methods, Materials, Models*, 2nd ed.; Heitjans, P., Kärger, J., Eds.; Springer: Berlin, 2005; p 367.
(26) Heitjans, P.; Indris, S.; Wilkening, M. *Diffusion Fundam.* **2005**, *2*, 45.
(27) Wilkening, M.; Iwaniak, W.; Heine, J.; Epp, V.; Kleinert, A.; Behrens, M.; Nuspl, G.; Bensch, W.; Heitjans, P. *Phys. Chem. Chem. Phys.* **2007**, *9*, 6199.
(28) Heitjans, P.; Wilkening, M. *MRS Bull.* **2009**, *34*, 915.
(29) Böhmer, R.; Jörg, T.; Qi, F.; Titze, A. *Chem. Phys. Lett.* **2000**, *316*, 419.
(30) Qi, F.; Jörg, T.; Böhmer, R. *Solid State Nucl. Magn. Reson.* **2002**, *22*, 484.
(31) Qi, F.; Rier, C.; Böhmer, R.; Franke, W.; Heitjans, P. *Phys. Rev. B* **2005**, *72*, 104301.
(32) Wilkening, M.; Heitjans, P. *J. Phys.: Condens. Matter* **2006**, *18*, 9849.
(33) Wilkening, M.; Küchler, W.; Heitjans, P. *Phys. Rev. Lett.* **2006**, *96*, 065901.
(34) Wilkening, M.; Amade, R.; Iwaniak, W.; Heitjans, P. *Phys. Chem. Chem. Phys.* **2007**, *9*, 1239.
(35) Wilkening, M.; Gebauer, D.; Heitjans, P. *J. Phys.: Condens. Matter* **2008**, *20*, 022201.
(36) Kuhn, A.; Wilkening, M.; Heitjans, P. *Solid State Ion.* **2009**, *180*, 302.
(37) Wilkening, M.; Heine, J.; Lyness, C.; Armstrong, A. R.; Bruce, P. G. *Phys. Rev. B* **2009**, *80*, 064302.
(38) Wilkening, M.; Lyness, C.; Armstrong, A. R.; Bruce, P. G. *J. Phys. Chem. C* **2009**, *113*, 4741.
(39) Carlier, D.; Ménétrier, M.; Grey, C. P.; Delmas, C.; Ceder, G. *Phys. Rev. B* **2003**, *67*.
(40) Burns, J. H.; Tennisse, A. C.; Brunton, G. D. *Acta Cryst. Sec. B* **1968**, *24*, 225.
(41) Duer, M. J. *Introduction to Solid-State NMR Spectroscopy*; Blackwell: Oxford, 2004.
(42) Fukushima, E.; Roeder, S. B. W. *Experimental Pulse NMR*; Addison-Wesley: Reading, 1981.
(43) Lee, Y. J.; Wang, F.; Grey, C. P. *J. Am. Chem. Soc.* **1998**, *120*, 12601.
(44) Armstrong, A. R.; Lyness, C.; Ménétrier, M.; Bruce, P. G. *Chem. Mater.* **2010**, *22*, 1892.

JP103433H